Journal of Computational Acoustics, Vol. 8, No. 1 (2000) 121–137


# ANALYTICAL AND NUMERICAL STUDIES OF A FINITE ELEMENT PML FOR THE HELMHOLTZ EQUATION

ISAAC HARARI and MICHAEL SLAVUTIN
*Department of Solid Mechanics, Materials and Structures*
*Tel Aviv University, 69978 Ramat Aviv, Israel*

ELI TURKEL
*School of Mathematical Sciences*
*Tel Aviv University, 69978 Ramat Aviv, Israel*

Received 3 June 1999
Revised 4 November 1999

A symmetric PML formulation that is suitable for finite element computation of time-harmonic acoustic waves in exterior domains is analyzed. Dispersion analysis displays the dependence of the discrete representation of the PML parameters on mesh refinement. Stabilization by modification of the coefficients is employed to improve PML performance, in conjunction with standard stabilized finite elements in the Helmholtz region. Numerical results validate the good performance of this finite element PML approach.

## 1. Introduction

The concept of a perfectly matched layer (PML) was conceived by Bérenger[1] as a tool for finite difference computation of time-dependent electromagnetic waves in unbounded domains. By splitting a scalar field into two nonphysical "components," the original PML equations describe decaying waves. Proper selection of the PML coefficients assures that the interface of such a region with a region governed by the standard Maxwell equations does not reflect plane waves at any angle of incidence. Bérenger later extended this formulation to three dimensions.[2]

The PML method rapidly gained immense popularity among practitioners in computational electromagnetics. A large body of literature contains alternative PML formulations and extensions of this concept to additional geometries and applications. Among these are an approach based on a Lorentz material model.[3] PML equations are also derived by introducing anisotropy,[4] instead of field splitting as in the original concept. This formulation is well-suited for finite element analysis. Alternatively, anisotropic properties may be obtained by a complex coordinate transformation.[5] This procedure is employed to extend the formulation to curvilinear coordinates.[6,7] The boundary conditions specified on the truncation boundary of the PML region seem to have little effect on performance.[7,8]

An alternative formulation is the uniaxial PML layer formulated by Gedney.[9,10] Some of these approaches are reviewed in Refs. 11 and 12. The method was also applied to computational acoustics.[13] This work examines an alternative approach, specific to time-harmonic acoustics and based on complex-valued anisotropic properties.[12]

While a great deal of numerical experience has accumulated, the understanding of the mathematical framework underlying this methodology seems to lag behind. Recent analysis indicates that the two-dimensional PML equations in their original form are ill posed due to a weak instability,[14] although little numerical evidence has been reported.

In this work, we study the properties of the finite element approximation of the PML equation for exterior problems of acoustics, presented in Sec. 2. A PML formulation with complex-valued anisotropic properties[12] is presented in Sec. 3. The discretized equations are analyzed in Sec. 4, and an improvement is proposed by means of modified coefficients. The performance of this method is tested numerically in Sec. 5 and compared to alternative techniques.

## 2. Exterior Boundary-Value Problem of Acoustics

Let $\mathcal{R} \subset \mathbb{R}^d$ be a $d$-dimensional unbounded region. The boundary of $\mathcal{R}$, denoted by $\Gamma$, is internal and assumed piecewise smooth (Fig. 1). The outward unit vector normal to $\Gamma$ is denoted by $\mathbf{n}$. We assume that $\Gamma$ admits the partition $\Gamma = \overline{\Gamma_g \bigcup \Gamma_h}$, where $\Gamma_g \bigcap \Gamma_h = \emptyset$.

We consider a boundary-value problem related to acoustic radiation and scattering governed by the Helmholtz equation: find $u: \overline{\mathcal{R}} \to \mathbb{C}$, the spatial component of the acoustic pressure or velocity potential, such that

$$-\mathcal{L}u = f \qquad \text{in } \mathcal{R} \tag{2.1}$$

$$u = p \qquad \text{on } \Gamma_g \tag{2.2}$$

$$\frac{\partial u}{\partial n} = ikv \qquad \text{on } \Gamma_h \tag{2.3}$$

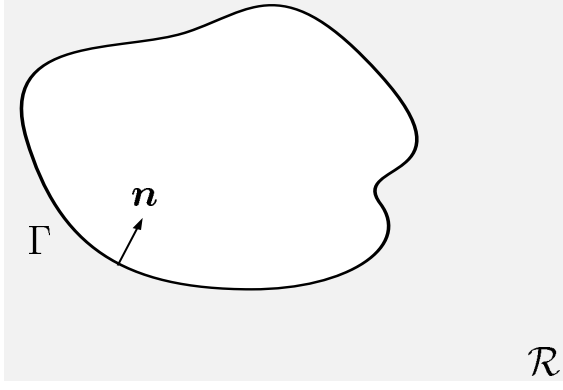


Fig. 1. An unbounded region with an internal boundary.

$$\lim_{r\to\infty} r^{\frac{d-1}{2}}\left(\frac{\partial u}{\partial r} + iku\right) = 0 \tag{2.4}$$

Here $\mathcal{L}u := \Delta u + k^2 u$ is the Helmholtz operator, $\Delta$ is the Laplace operator and $k \in \mathbb{C}$ is the wave number, $\operatorname{Im} k \geq 0$; $\partial u/\partial n := \nabla u \cdot \mathbf{n}$ is the normal derivative and $\nabla$ is the gradient operator; $i = \sqrt{-1}$ is the imaginary unit; $r$ is the distance from the origin; and $f\colon \mathcal{R} \to \mathbb{C}$, $p\colon \Gamma_g \to \mathbb{C}$ and $v\colon \Gamma_h \to \mathbb{C}$ are the prescribed data.

Equation (2.4) is the *Sommerfeld radiation condition* and allows only outgoing waves at infinity. The radiation condition requires that energy flux at infinity be positive, thereby guaranteeing that the solution to the boundary-value problem (2.1)–(2.4) is unique (see pp. 296–299 in Stakgold[15] and pp. 55–60 in Wilcox,[16] and references therein). It can be shown that the PML layer enforces the Sommerfeld radiation condition.[17] Appropriate representation of this condition is crucial to the reliability of any numerical formulation of the problem (2.1)–(2.4). This form of the radiation condition, by which outgoing waves are of the form $\exp(-ikr)$ is adopted for consistency with common PML notation.

## 3. PML Formulation

The PML equations were originally formulated for the time-dependent Maxwell equations by employing auxiliary fields.[1] This formulation was later applied to the Helmholtz equation, replacing the auxiliary fields by complex-valued coefficients.[12] Based on this approach, the PML equation for two-dimensional time-harmonic acoustics can be written as

$$\left(\frac{K_y}{K_x}u_{,x}\right)_{,x} + \left(\frac{K_x}{K_y}u_{,y}\right)_{,y} + K_x K_y u = 0 \tag{3.1}$$

where

$$K_x = k - i\sigma_x(x) \tag{3.2}$$

$$K_y = k - i\sigma_y(y) \tag{3.3}$$

The equation reduces to Helmholtz when $\sigma_x = \sigma_y = 0$. The coefficients $\sigma_x$ and $\sigma_y$ are usually taken to vary from a value of zero at the interface (for the "perfect match") to a maximal value at the truncation of the layer. In the layers to the right and left of the physical domain $\sigma_y = 0$ and similarly on the top and bottom layers $\sigma_x = 0$. Only in corner regions are both $\sigma_x$ and $\sigma_y$ nonzero.

In abstract notation we write

$$\nabla \cdot (\mathbf{D}\nabla u) + K_x K_y u = 0 \tag{3.4}$$

where

$$\mathbf{D} = \begin{bmatrix} \dfrac{K_y}{K_x} & 0 \\ 0 & \dfrac{K_x}{K_y} \end{bmatrix} \tag{3.5}$$

Note that $\mathbf{D}$ is symmetric (but not Hermitian) and $\det \mathbf{D} = 1$. However, $\mathbf{D}$ can be made truly symmetric by choosing as the unknown variables $(\mathrm{Re}(u), -\mathrm{Im}(u))$.

A weak form of the Dirichlet problem is to find $u$, such that $\forall\, w$ (weighting functions that satisfy $w = 0$ on the boundary)

$$\int_\Omega (\nabla w \cdot \mathbf{D} \nabla u - w K_x K_y u)\, d\Omega = 0 \tag{3.6}$$

(The treatment of other boundary conditions is straightforward.)

Incorporating the PML approach in finite element analysis has several implementational ramifications:

(i) The PML interface is frequently a rectangle in two dimensions, easily fitting around slender bodies that are often of interest in naval and aerospace applications. Furthermore, interfaces need not be closed surfaces. For example, the computation of unbounded wave guides does not require special treatment. In contrast, competing approaches such as nonreflecting boundary conditions and infinite elements often employ closed circular interfaces. The consideration of elongated geometries and open interfaces then requires additional treatment.[18,19]

(ii) The PML equation is fully compatible with element-based data structures typical of finite elements. Standard programming techniques and efficient solution algorithms that exploit the special structure of the coefficient matrices may be employed. Again, this is in contrast to several approaches that couple degrees of freedom on the interface.

(iii) The PML approach increases the size of the coefficient matrices considerably due to the need to discretize the PML region. This drawback may entirely offset the advantageous effect of the special structure of the matrices on the cost of computation. This important issue requires further investigation that is beyond the scope of the current work.

## 4. Analysis

The justification for employing the PML technique for domain-based computation of exterior problems stems from analysis of its performance on *continuous* forms of the problem. In particular, plane waves at any angle of incidence are not reflected from PML interfaces (with properly chosen coefficients),[1,2] and waves decay in the PML region so that there is essentially no adverse effect from truncating the PML region itself. The degree to which these properties are retained after discretization has not been studied sufficiently.

On a uniform $d$-dimensional mesh in the PML region, when the wave number is constant the finite element representation of the propagation of a plane wave along the mesh lines perpendicular to the interface is identical to the one-dimensional problem. Similar analyses may be performed for other directions of propagation. In those cases, one needs to assume the orientation of the mesh with respect to the direction of propagation. Dispersion may then be analyzed and corrected in a manner similar to the analysis performed in the following for propagation along mesh lines.[20,21]

In general, the direction of propagation is unknown in advance. We expect results of the analysis of propagation along mesh lines to be useful even for these cases. Numerical results support this conjecture. Consequently, we analyze the one-dimensional case. In this case $\sigma_y = 0$. For simplicity we denote $\sigma = \sigma_x$ and $K = k - i\sigma$, and the PML equation is

$$\left(\frac{u'}{K}\right)' + Ku = 0 \tag{4.1}$$

An outgoing solution to this equation is[22]

$$u = \exp\left(-i\int_0^x K(\xi)\,d\xi\right) \tag{4.2}$$

### 4.1. *Dispersion*

The first step in characterizing the PML formulation is to determine its dispersion properties, following the procedure for finite elements with the Helmholtz equation.[20,23–26] Dispersion analyses are usually performed for homogeneous media. In this case we consider $K$ to be a constant in an unbounded PML region.

Consider a uniform one-dimensional mesh of linear elements of length $h$ with nodal points at $x_A = Ah$. Values of the outgoing exact solution (4.2) at the nodal points are

$$u(x_A) = (\exp(-iKh))^A \tag{4.3}$$

Corresponding nodal values of the finite element solution are

$$u_A = (\exp(-iK^h h))^A \tag{4.4}$$

where $u_A = u^h(x_A)$ and $K^h = k^h - i\sigma^h$. Here, $k^h$ and $\sigma^h$, the approximations of $k$ and $\sigma$, respectively, are determined by the following dispersion analysis.

We consider a general lumping of the lower order term

$$\frac{-u_{A-1} + 2u_A - u_{A+1}}{Kh} - Kh(\alpha u_{A-1} + (1-2\alpha)u_A + \alpha u_{A+1}) = 0 \tag{4.5}$$

For $\alpha = 1/12$ this gives a fourth order scheme.[27,28] For $\alpha = 1/6$ this is equivalent to finite elements using linear elements. The finite element equation at interior node $A$ reduces to

$$\frac{-u_{A-1} + 2u_A - u_{A+1}}{Kh} - Kh\frac{u_{A-1} + 4u_A + u_{A+1}}{6} = 0 \tag{4.6}$$

By (4.4) this yields

$$\begin{aligned} 0 &= \left(1 + \frac{(Kh)^2}{6}\right) \Big/ \exp(-iK^h h) - 2\left(1 - \frac{(Kh)^2}{3}\right) + \left(1 + \frac{(Kh)^2}{6}\right)\exp(-iK^h h) \\ &= 2\left(1 + \frac{(Kh)^2}{6}\right)\cos(K^h h) - 2\left(1 - \frac{(Kh)^2}{3}\right) \end{aligned} \tag{4.7}$$

Thus, the finite element dispersion relation in the PML region

$$K^h h = \arccos\left(\frac{1-(Kh)^2/3}{1+(Kh)^2/6}\right)$$
$$= Kh - \frac{1}{24}(Kh)^3 + \frac{3}{640}(Kh)^5 - \frac{103}{193536}(Kh)^7 + O((Kh)^9) \tag{4.8}$$

is identical in form to the finite element dispersion relation in the standard acoustic region (for $k^h h$ in terms of $kh$). This relation may be parameterized in terms of wave resolution, the number of nodes per wavelength, $G = 2\pi/(kh)$, and either $\sigma h$ or $\sigma/k$. The dispersion relation (4.8) can be written in more explicit form

$$\cos(k^h h)\cosh(\sigma^h h) = \frac{1-2a^2-a-2b^2}{1+2a+a^2+b^2} \tag{4.9}$$

$$\sin(k^h h)\sinh(\sigma^h h) = \frac{3b}{1+2a+a^2+b^2} \tag{4.10}$$

where

$$a = \frac{(kh)^2-(\sigma h)^2}{6} \tag{4.11}$$

$$b = (kh)(\sigma h)/3 \tag{4.12}$$

Figure 2 shows the discrete representations of the wave number $k^h$ and decay rate $\sigma^h$. Note the reduction in the relative value of the decay rate at low wave resolutions.

The value of $\sigma$ on the interface with the standard acoustic region is zero. The curve in the $\sigma = 0$ plane of the left figure depicts the standard acoustic finite element dispersion relation

$$k^h h = \arccos\left(\frac{1-(kh)^2/3}{1+(kh)^2/6}\right) \tag{4.13}$$

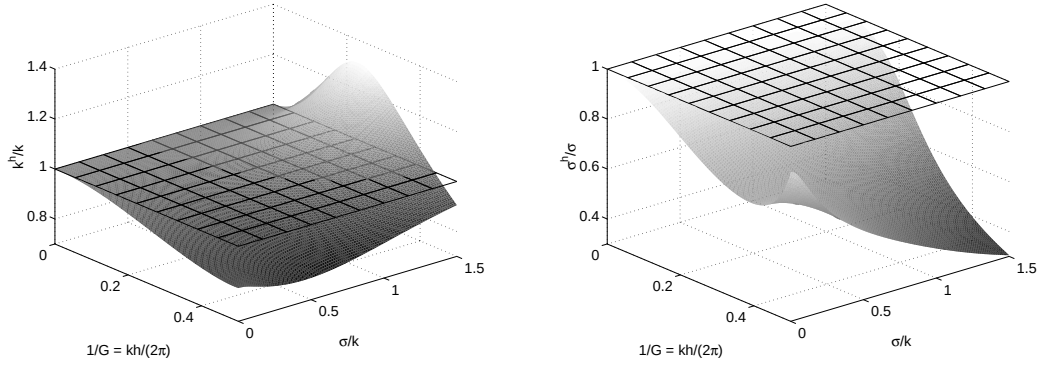


Fig. 2. Discrete representations of the wave number (left) and decay rate for constant coefficient $K$.

Numerical dispersion of discrete formulations gives rise to spurious reflection at transitions in wave resolution.[20] The fact that the dispersion relation is identical on the interface of the acoustic and PML regions suggests that the meshing of the PML region should maintain the same resolution as the outer parts of the standard acoustic region, to reduce spurious reflection at the interface.

### 4.2. *Stabilization*

Spurious dispersion in the computation is related to the pollution effect, in which numerical solutions of the Helmholtz equation differ significantly from the best approximation,[29] leading to loss of guaranteed performance at any mesh refinement. Many approaches to alleviating this difficulty, often referred to as stabilization, have been proposed, usually based on modifications of the classical Galerkin method. Among these methods are: Galerkin/least-squares[20] and generalizations there-of,[30] residual-free bubbles,[31] and variational multiscale.[32]

While accuracy in the PML region is of little consequence, reflection from its truncation should be minimized, and the interaction of PML with stabilized finite elements is of interest. In the following, we propose a rudimentary approach to stabilization of the PML formulation, based on concepts that arise in Galerkin/least-squares. We exploit the absence of sources in the PML region, and the structured meshing typical of most applications. This allows us to define simple modifications of the wave number and decay rate, that are applicable to linear elements for problems in which the physical wave number is constant. The modifications are based on the dispersion analysis of Sec. 4.1, for a constant PML coefficient on a uniform mesh in one dimension, yet the results may be applied to typical implementations of PML with varying coefficients, on nonuniform meshes in multi-dimensional configurations.

On a uniform mesh of linear elements, the Galerkin/least-squares stabilization of the constant-coefficient, homogeneous Helmholtz equation may also be obtained by modifying the wave number. (Similar improvements have been obtained in finite differences by generalized definitions of derivatives.[27]) We design a modified wave number approach for PML that is motivated by the Galerkin/least-squares method. This simplistic approach lacks the generality of Galerkin/least-squares for higher-order elements and unstructured meshes, yet it is easy to implement. The PML parameter $K$ $(= k - i\sigma)$ is replaced by a modified coefficient $\widetilde{K}$ that is defined so that the approximation $K^h$ in (4.5) is exact, namely

$$\widetilde{K}h = \sqrt{\frac{2(1-\cos(Kh))}{2\alpha\cos(Kh) + 1 - 2\alpha}} \tag{4.14}$$

Nehrbass[33] modified the coefficient to achieve higher-order phase error rather than making it exact. For the finite element method (4.6) this reduces to

$$\tilde{K}h = \sqrt{6\frac{1-\cos(Kh)}{2+\cos(Kh)}} \tag{4.15}$$

Modifications of $k$ and $\sigma$ are obtained as the real and imaginary parts of $\widetilde{K}$, respectively. The modification is consistent in the sense that

$$\lim_{h\to 0} \tilde{K} = K \tag{4.16}$$

We also note that $\lim_{\sigma h\to\infty} \widetilde{K}h = -\sqrt{6}i$. This gives an indication of the numerical values of the modified parameters for large values of the decay rate, which may occur at the truncation of the PML region. The proposed stabilization scheme thus consists of employing the modified parameters in the PML region, and standard stabilized finite elements in the Helmholtz region.

### 4.3. *Simple example: linearly-varying PML coefficient*

To demonstrate the improvement obtained by modifying the coefficient, consider the simple problem

$$\begin{aligned} u'' + k^2 u = 0 \qquad & -1 < x < \infty \\ u(-1) = \exp(ik) \qquad & \\ \lim_{x\to\infty} u' + iku = 0 \qquad & \end{aligned} \tag{4.17}$$

The solution is

$$u = \exp(-ikx) \tag{4.18}$$

We compute the solution (4.6) with $k = 12$ in the interval $-1 < x < 0$. The PML region is taken as $0 < x < 0.2$, and the PML coefficient $\sigma$ varies linearly from zero at the interface to a maximal value of 50. The mesh size is uniform, $h = 0.1$, for a resolution of approximately

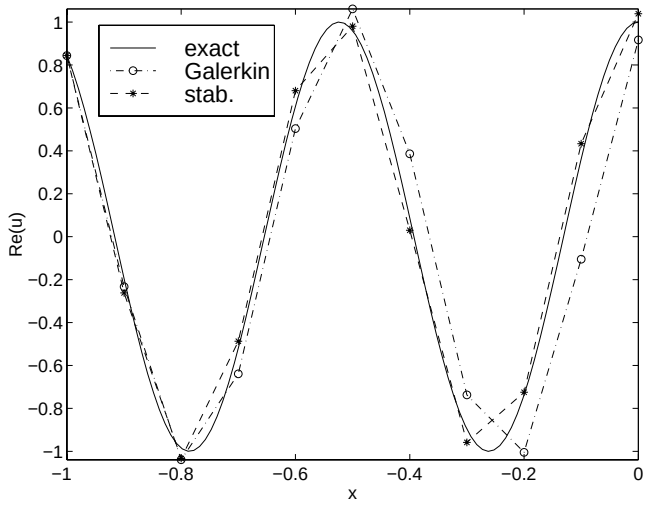


Fig. 3. Solution of simple example with linearly-varying PML coefficient.

five points per wavelength (recall, $G = 2\pi/(kh)$). The standard finite element solution, denoted Galerkin, is compared in Fig. 3 to the stabilized solution in which the Helmholtz region is modified according to Galerkin/least-squares and the treatment of the PML region follows the modifications proposed in Sec. 4.2. The improvement obtained by the stabilized approach, even for this case with a varying PML coefficient, is evident.

## 5. Numerical Results

Numerical results of PML formulations are compared to exact and DtN solutions. The DtN method is a general scheme for handling boundary-value problems in unbounded domains. The method for general linear elliptic problems was developed by Givoli and Keller[34,35] and is related to similar work in acoustics.[36,37] The DtN method introduces artificial boundaries (typically spherical) to form bounded computational domains that are suitable for domain-based discretization. Correct far-field behavior is enforced by specifying proper boundary conditions on this boundary. The DtN map is usually expressed in the form of an infinite series. In practice the map is approximated by truncating the series, so that it is based on a representation that is not complete. Uniqueness of solutions to two- and three-dimensional problems is guaranteed by selecting the number of terms in the truncated DtN map so that it is no less than $kR$, where $R$ is the radius of the artificial boundary.[38,39] DtN boundary conditions can be very accurate, but all of the degrees of freedom on the artificial boundary are coupled, potentially increasing the cost of computation.

### 5.1. *Wave guide*

We consider a wave guide in two dimensions, represented by a semi-infinite strip of constant width $b = \pi$, aligned along the positive $x$-axis with walls at $y = 0$ and $y = \pi$. Homogeneous Dirichlet boundary conditions are specified at the walls. The radiation condition (2.4) is replaced by the condition that $u$ is bounded and does not contain incoming waves at $x \to \infty$. (Radiation conditions for wave guides are treated rigorously elsewhere.[17,40]) The boundary $x = 0$ is a radiating wall with

$$u(0, y) = c_1 \sin(\ell_1 y) + c_2 \sin(\ell_2 y), \qquad 0 < y < \pi \tag{5.1}$$

Here $c_1$ and $c_2$ are given constants, and $\ell_1$ and $\ell_2$ are given integers that satisfy $\ell_1 < k < \ell_2$. The exact solution is composed of a propagating and an evanescent wave

$$u = c_1 \exp\left(-i\sqrt{k^2 - \ell_1^2}\, x\right) \sin(\ell_1 y) + c_2 \exp\left(-\sqrt{\ell_2^2 - k^2}\, x\right) \sin(\ell_2 y) \tag{5.2}$$

For finite element computation, the wave guide is truncated at $x = 5\pi$ (Fig. 4). The resulting computational domain is meshed with $50 \times 10$ square, bilinear elements, so that the element length is uniform ($h = b/10$). The PML region is parallel to the $y$-axis, starting at $x = 5\pi$, with 10 elements in the direction transverse to the layer. The PML parameter $\sigma_x(x)$ varies quadratically from a value of zero at the interface to 40 at the outer edge of the layer, and $\sigma_y = 0$.

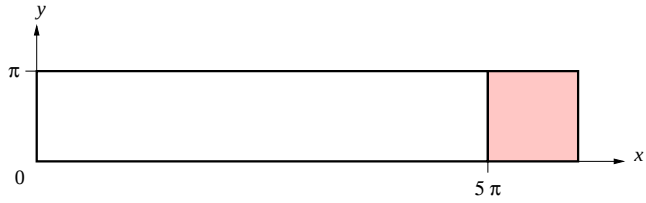


Fig. 4. Wave guide with PML.

The problem is solved by Gauss elimination with $kb = 1.25\pi$ (a resolution of 16 points per wavelength), $\ell_1 = 1$, $\ell_2 = 2$, $c_1 = 2$ and $c_2 = 1$. The contours in Fig. 5 show that the absorbing layer performs well. The evanescent wave produces a lack of symmetry near the radiating wall, which decays further along the wave guide. The numerical dispersion of standard finite elements is relatively small at this resolution, yet it leads to the increasing error evident in the propagating wave along the wave guide.

In order to emphasize the deleterious effects of numerical dispersion, consider the *degenerate* case in which $\ell_1 = k$ ($c_2 = 0$). The exact solution is constant along the wave guide. The problem is solved with $kb = \pi$ (20 points per wavelength) and $c_1 = 1$, so that the exact solution is real valued. Figure 6 shows the solution along the axis of the wave guide ($y = \pi/2$). The standard finite element solution (by the Galerkin method) exhibits strong decay in the real part (bold line) due to numerical dispersion, along with an imaginary part that does not exist in the exact solution. Stabilization by the Galerkin/least-squares method in the Helmholtz region and the modifications proposed in Sec. 4.2 in the PML region reduces numerical dispersion and improves the results significantly. This example demonstrates the potential of exploiting existing concepts of stabilized finite element methodology to improve the performance of PML finite elements.

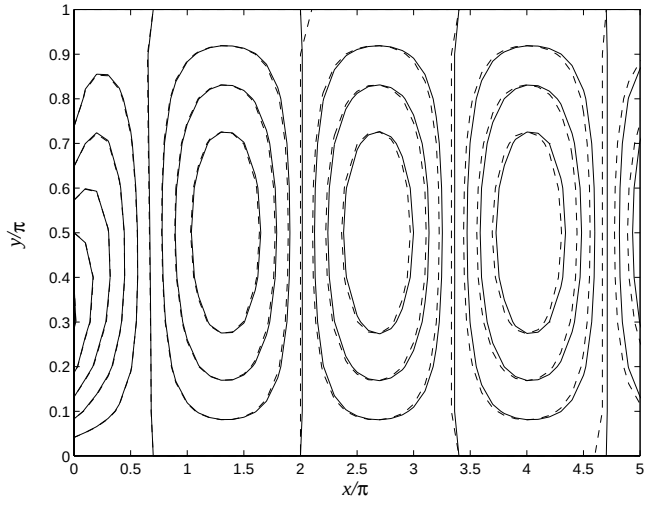


Fig. 5. Real part of the wave guide solution $kb = 1.25\pi$ (exact solution is dashed).

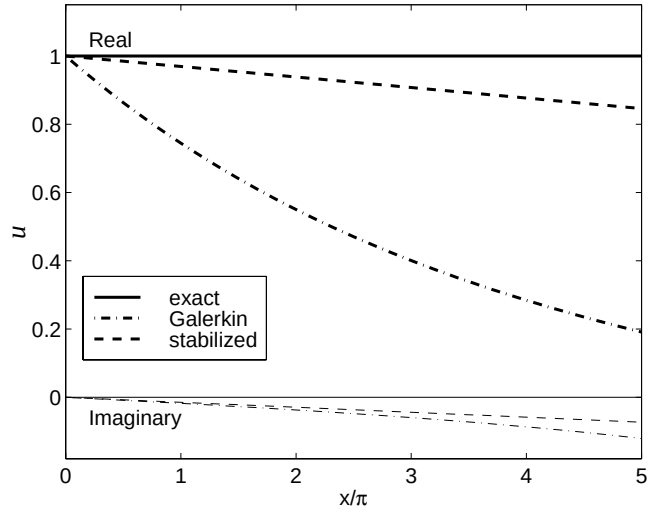


Fig. 6. Real (bold lines) and imaginary parts of degenerate wave guide solutions along the axis $y = \pi/2$.

### 5.2. *Circumferentially harmonic radiation from a cylinder*

In the following, numerical results are presented for exterior problems bounded internally by an infinite circular cylinder of radius $a$. Soft (Dirichlet) boundary conditions are specified on the wet surface ($r = a$) to represent a pressure-release cylinder.

The cylinder is centered within the computational domain. For finite element computation with PML, the computational domain is a square of side $2a$. The finite element mesh employed, composed of approximately 560 elements, is shown in Fig. 7 (left). The PML region surrounds the finite element domain with strips of ten elements of length 0.1 in the width of each strip, adding 1,200 elements to the mesh, increasing the cost of directly solving

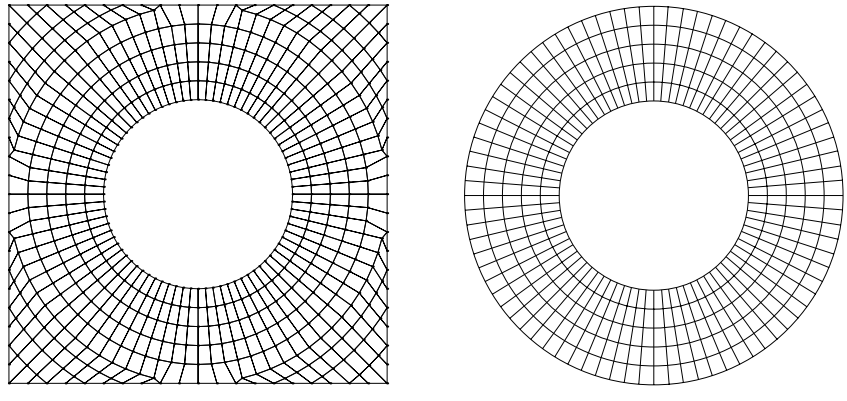

Fig. 7. The computational domain exterior to a cylinder of radius $a$ with: a square PML interface of side $2a$ (left); a circular DtN interface at $R = 2a$, discretized by $5 \times 80$ linear quadrilateral finite elements (right).

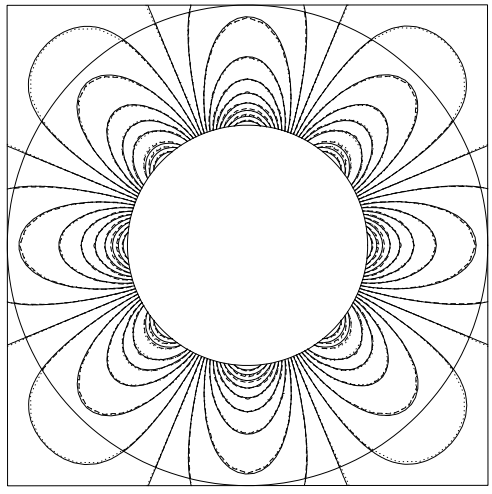

Fig. 8. Circumferentially harmonic ($n = 4$) radiation from a cylinder of radius $a$, $ka = 2$, $\sim 16$ points per wavelength (solid contours denote exact solution, dotted contours denote PML, and dashed contours denote DtN, $N = 10$).

the equations by more than an order of magnitude. On the PML strips parallel to the $x$-axis $\sigma_x = 0$, and $\sigma_y(y)$ varies quadratically from a value of 0 at the interface to 30 at the outer edge of the layer. On the strips parallel to the $y$-axis $\sigma_y = 0$, and $\sigma_x(x)$ varies quadratically from 0 to 30. In the corners, both parameters are varied appropriately. From here on, no stabilization is employed.

The circular artificial boundary of the DtN formulation is located at $R = 2a$. The computational domain is discretized by $5 \times 80$ bilinear quadrilateral finite elements (Fig. 7, right). The global DtN boundary conditions couple all of the degrees of freedom on the artificial boundary, increasing the bandwidth of the matrix equations, and consequently the computational cost rises, again by more than an order of magnitude for direct solvers.

Consider a cylinder with circumferentially harmonic loading. For a load distribution $\cos n\theta$, the normalized exact solution is $u = H_n^{(1)}(kr)\cos n\theta / H_n^{(1)}(ka)$. We examine the problem with a geometrically nondimensionalized wave number $ka = 2$ (the wavelength is about one and a half times the diameter of the cylinder and three times the width of the domain), and a typical resolution of approximately 16 nodal points per wavelength in the finite element meshes (Fig. 7).

We consider the fifth circumferential mode, $n = 4$. Figure 8 shows the real part of the analytical and numerical solutions, for the PML and the DtN formulations (with 10 terms in the DtN operator, sufficient for uniqueness). Both computations clearly represent the main features of the analytical solution. Note that DtN condition itself (with $N = 10$) is exact for this problem, and the error is due to finite element discretization in the domain and approximation of the DtN condition on the interface. The PML elements are not an exact representation of the radiation condition, but the results are comparable to DtN.

### 5.3. *Radiation from a sector of a cylinder*

We consider the nonuniform radiation from an infinite circular cylinder with a constant inhomogeneous value on an arc ($-\alpha < \theta < \alpha$) and vanishing elsewhere, so that there are two points of discontinuity in the boundary data. The normalized analytical solution to this problem for a cylinder of radius $a$ is

$$u = \frac{2}{\pi} {\sum_{n=0}^{\infty}}' \frac{\sin n\alpha}{n} \frac{H_n^{(1)}(kr)}{H_n^{(1)}(ka)} \cos n\theta \tag{5.3}$$

The prime on the sum indicates that the first term is halved. For low wave numbers this solution is relatively uniform in the circumferential direction. The directionality of the solution grows as the wave number is increased, and the solution becomes attenuated at the side of the cylinder opposite the radiating element.

Numerical results of PML formulations for this problem are compared to Trefftz infinite element (TIE) solutions, in addition to exact and DtN solutions. The term infinite elements refers to a class of methods which is based on interpolation with suitable behavior in the complement of the computational domain.[18,41–44] In contrast to global DtN boundary conditions, infinite elements retain the element-based data structure of finite elements, thus preserving the bandedness of the discrete equations. The Trefftz infinite elements employed in the following are developed by a novel approach to exterior problems of time-harmonic acoustics.[45] This approach is based on a variational framework for finite element computation in unbounded domains.[46] Weakly coupling inner fields to outgoing outer field representations that satisfy the Helmholtz equation yields problems on bounded domains. This treatment of the outer field is in the framework of the Trefftz approach.[47] The computational

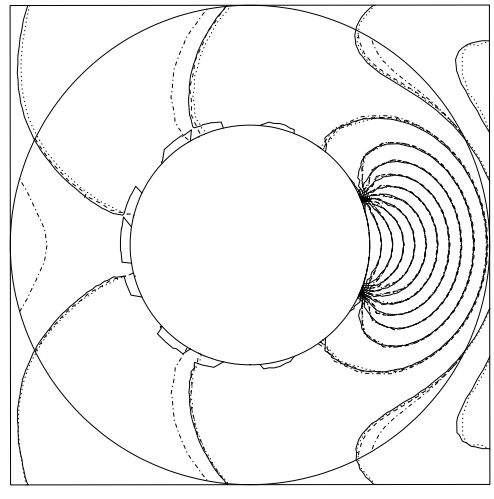

Fig. 9. Radiation from a sector of a cylinder of radius $a$, $ka = 2$, $\sim 16$ points per wavelength (solid contours denote analytical solution (5.3), dotted contours denote PML, dashed contours denote DtN, $N = 10$, and dash-dotted contours denote TIE).

Table 1. Relative errors for radiation from a sector of a cylinder of radius $a$, ($ka = 2$, $\sim 16$ points per wavelength).

| Method | $\frac{\lvert u^h - u^{\mathrm{I}}\rvert_1}{\lvert u^{\mathrm{I}}\rvert_1}[\%]$ |
|---|---|
| PML | 8.6 |
| DtN | 9.6 |
| TIE | 9.8 |

domain of the infinite element formulation is formed by a circular interface, and, as in DtN, is located at $R = 2a$ (Fig. 7).

We select $\alpha = \pi/8$. Figure 9 shows the real part of the analytical and numerical solutions (without stabilization), for the PML, DtN (with ten terms in the operator), and TIE formulations (of lowest order). The low-amplitude oscillations of the *analytical* solution in the vicinity of the wet surface are merely an artifact of the truncated series representation (60 terms) of the discontinuity in the boundary data, and are not relevant to the validation of the numerical results. The numerical solutions capture the essential physics of the problem, without visible reflection from the interfaces.

Errors relative to the interpolation of the analytic solution $u^{\mathrm{I}}$, measured in the $H_1$ seminorm, are presented in Table 1. Despite the noticeable deviations of the TIE contours from those of the other methods in parts of the domain (Fig. 9), the global error is similar. This is due to the fact that the errors in the vicinity of the boundary data discontinuities dominate in all methods, and contributions of errors on other regions, where solutions vary slowly, are much smaller.

## 6. Conclusions

The performance of a PML finite element method for solving exterior problems of time-harmonic acoustics is examined in this work. The PML approach easily accommodates elongated geometries and open boundaries, retaining the element-based data structure of finite elements. The computational efficiency of this approach in comparison to competing techniques requires further investigation.

The dispersion analysis in this work is restricted to plane waves at normal incidence to the interface of an unbounded PML region with a constant coefficient. A degradation in the discrete representation of the PML decay rate is observed. The finite element dispersion properties at the interface are identical to those in the standard acoustic region. This suggests keeping the mesh uniform, and at a resolution similar to that of the acoustic region in the vicinity of the interface, in order to reduce spurious reflection.

A simplistic approach to improved performance by stabilization exploits the structured meshes and absence of sources in typical PML implementations. Stabilization for linear

elements is then attained by modifying the coefficients. This approach is applicable to layers with varying coefficients in multi-dimensional configurations.

Numerical results validate the good performance of this finite element PML approach to exterior problems of time-harmonic acoustics. Several problems are examined. PML results compare favorably to analytical solutions, as well as to computation with DtN boundary conditions and Trefftz infinite elements.

## Acknowledgments

The authors wish to thank Paul Barbone for helpful discussions.

## References

1. J.-P. Bérenger, "A perfectly matched layer for the absorption of electromagnetic waves," *J. Comput. Phys.* **114**(2) (1994), 185–200.
2. J.-P. Bérenger, "Three-dimensional perfectly matched layer for the absorption of electromagnetic waves," *J. Comput. Phys.* **127**(2) (1996), 363–379.
3. R. W. Ziolkowski, "Time-derivative Lorentz material model-based absorbing boundary condition," *IEEE Trans. Antennas Propagat.* **45**(10) (1997), 1530–1535.
4. J.-Y. Wu, D. M. Kingsland, J.-F. Lee, and R. Lee, "A comparison of anisotropic PML to Berenger's PML and its application to the finite-element method for EM scattering," *IEEE Trans. Antennas Propagat.* **45**(1) (1997), 40–50.
5. F. L. Teixeira and W. C. Chew, "A general approach to extend Berenger's absorbing boundary condition to anisotropic and dispersive media," *IEEE Trans. Antennas Propagat.* **46**(9) (1998), 1386–1387.
6. F. Collino and P. Monk, "The perfectly matched layer in curvilinear coordinates," *SIAM J. Sci. Comput.* **19**(6) (1998), 2061–2090.
7. F. Collino and P. B. Monk, "Optimizing the perfectly matched layer," *Comput. Meths. Appl. Mech. Eng.* **164**(1–2) (1998), 157–171.
8. P. G. Petropoulos, "On the termination of the perfectly matched layer with local absorbing boundary conditions," *J. Comput. Phys.* **143**(2) (1998), 665–673.
9. S. D. Gedney, "An anisotropic perfectly matched layer-absorbing medium for the truncation of FDTD lattices," *IEEE Trans. Antennas Propagat.* **44**(12) (1996), 1630–1639.
10. J. A. Roden and S. D. Gedney, "Efficient implementation of the uniaxial-based PML media in three-dimensional nonorthogonal coordinates with the use of the FDTD technique," *Microw. Opt. Technol. Lett.* **14**(2) (1997), 71–75.
11. S. D. Gedney, "The perfectly matched layer absorbing medium," *Advances in Computational Electrodynamics*, ed. A. Taflove (Artech House Inc., Boston, MA, 1998), pp. 263–343.
12. E. Turkel and A. Yefet, "Absorbing PML boundary layers for wave-like equations," *Appl. Numer. Math.* **27**(4) (1998), 533–557.
13. Q. Qi and T. L. Geers, "Evaluation of the perfectly matched layer for computational acoustics," *J. Comput. Phys.* **139**(1) (1998), 166–183.
14. S. S. Abarbanel and D. Gottlieb, "A mathematical analysis of the PML method," *J. Comput. Phys.* **134**(2) (1997), 357–363.
15. I. Stakgold, *Boundary Value Problems of Mathematical Physics*, Volume II (The Macmillan Co., New York, 1968).
16. C. H. Wilcox, *Scattering Theory for the d'Alembert Equation in Exterior Domains* (Springer-Verlag, Berlin, 1975).

17. S. V. Tsynkov and E. Turkel, "A Cartesian perfectly matched layer for the Helmholtz equation," *Artificial Boundary Conditions, with Applications to CFD Problems*, ed. L. Tourrette (Nova Science Publishers Inc., Commack, NY, 2000).
18. D. S. Burnett, "A three-dimensional acoustic infinite element based on a prolate spheroidal multipole expansion," *J. Acoust. Soc. Am.* **96**(5) (1994), 2798–2816.
19. I. Harari, I. Patlashenko, and D. Givoli, "Dirichlet-to-Neumann maps for unbounded wave guides," *J. Comput. Phys.* **143**(1) (1998), 200–223.
20. I. Harari, "Reducing spurious dispersion, anisotropy and reflection in finite element analysis of time-harmonic acoustics," *Comput. Meths. Appl. Mech. Eng.* **140**(1–2) (1997), 39–58.
21. L. L. Thompson and P. M. Pinsky, "A Galerkin least-squares finite element method for the two-dimensional Helmholtz equation," *Int. J. Num. Meth. Eng.* **38**(3) (1995), 371–397.
22. S. S. Abarbanel and D. Gottlieb, "On the construction and analysis of absorbing layers in CEM," *Appl. Num. Math.* **27**(4) (1998), 331–340.
23. N. N. Abboud and P. M. Pinsky, "Finite element dispersion analysis for the three-dimensional second-order scalar wave equation," *Int. J. Num. Meth. Eng.* **35**(6) (1992), 1183–1218.
24. K. Grosh and P. M. Pinsky, "Complex wave-number dispersion analysis of Galerkin and Galerkin least squares methods for fluid-loaded plates," *Comput. Meths. Appl. Mech. Eng.* **113**(1–2) (1994), 67–98.
25. I. Harari and T. J. R. Hughes, "Finite element methods for the Helmholtz equation in an exterior domain: Model problems," *Comput. Meths. Appl. Mech. Eng.* **87**(1) (1991), 59–96.
26. F. Ihlenburg and I. Babuška, "Dispersion analysis and error estimation of Galerkin finite element methods for the Helmholtz equation," *Int. J. Num. Meth. Eng.* **38**(22) (1995), 3745–3774.
27. I. Harari and E. Turkel, "Accurate finite difference methods for time-harmonic wave propagation," *J. Comput. Phys.* **119**(2) (1995), 252–270.
28. I. Singer and E. Turkel, "High order finite difference methods for the Helmholtz equation," *Comput. Meths. Appl. Mech. Eng.* **163** (1998), 343–358.
29. I. Babuška, F. Ihlenburg, E. T. Paik, and S. A. Sauter, "A generalized finite element method for solving the Helmholtz equation in two dimensions with minimal pollution," *Comput. Meths. Appl. Mech. Eng.* **128**(3–4) (1995), 325–359.
30. A. A. Oberai and P. M. Pinsky, "A residual-based finite element method for the Helmholtz equation," *Int. J. Num. Meth. Eng.* (1999) Submitted.
31. L. P. Franca and A. Russo, "Unlocking with residual-free bubbles," *Comput. Meths. Appl. Mech. Eng.* **142**(3–4) (1997), 361–364.
32. T. J. R. Hughes, "Multiscale phenomena: Green's functions, the Dirichlet-to-Neumann formulation, subgrid scale models, bubbles and the origins of stabilized methods," *Comput. Meths. Appl. Mech. Eng.* **127**(1–4) (1995), 387–401.
33. J. W. Nehrbass, J. O. Jevtic, and R. Lee, "Reducing the phase error for finite-difference methods without increasing the order," *IEEE Trans. Antennas Propagat.* **46**(8) (1998), 1194–1201.
34. D. Givoli and J. B. Keller, "A finite element method for large domains," *Comput. Meths. Appl. Mech. Eng.* **76**(1) (1989), 41–66.
35. J. B. Keller and D. Givoli, "Exact nonreflecting boundary conditions," *J. Comput. Phys.* **82**(1) (1989), 172–192.
36. K. Feng, "Asymptotic radiation conditions for reduced wave equation," *J. Comput. Math.* **2**(2) (1984), 130–138.
37. M. Masmoudi, "Numerical solution for exterior problems," *Numer. Math.* **51**(1) (1987), 87–101.
38. I. Harari and T. J. R. Hughes, "Analysis of continuous formulations underlying the computation of time-harmonic acoustics in exterior domains," *Comput. Meths. Appl. Mech. Eng.* **97**(1) (1992), 103–124.

39. I. Harari and T. J. R. Hughes, "Studies of domain-based formulations for computing exterior problems of acoustics," *Int. J. Num. Meth. Eng.* **37**(17) (1994), 2935–2950.
40. A. I. Nosich and V. P. Shestopalov, "Radiation conditions and uniqueness theorems for open waveguides," *Soviet J. Comm. Tech. Electron.* **34**(7) (1989), 107–115.
41. R. J. Astley, G. J. Macaulay, and J.-P. Coyette, "Mapped wave envelope elements for acoustical radiation and scattering," *J. Sound Vib.* **170**(1) (1994), 97–118.
42. P. Bettess, "Infinite elements," *Int. J. Num. Meth. Eng.* **11**(1) (1977), 53–64.
43. K. Gerdes and L. Demkowicz, "Solution of 3D-Laplace and Helmholtz equations in exterior domains using *hp*-infinite elements," *Comput. Meths. Appl. Mech. Eng.* **137**(3–4) (1996), 239–273.
44. O. C. Zienkiewicz, K. Bando, P. Bettess, C. Emson, and T. C. Chiam, "Mapped infinite elements for exterior wave problems," *Int. J. Num. Meth. Eng.* **21**(7) (1985), 1229–1251.
45. I. Harari, P. E. Barbone, M. Slavutin, and R. Shalom, "Boundary infinite elements for the Helmholtz equation in exterior domains," *Int. J. Num. Meth. Eng.* **41**(6) (1998), 1105–1131.
46. I. Harari, "A unified variational approach to domain-based computation of exterior problems of time-harmonic acoustics," *Appl. Num. Math.* **27**(4) (1998), 417–441.
47. J. Jirousek and A. Wróblewski, "*T*-elements: State of the art and future trends," *Arch. Comput. Methods Engrg.* **3**(4) (1996), 323–434.